Design of reverse transcriptase–specific nucleosides to visualize early steps of HIV-1 replication by click labeling

Received for publication, December 16, 2018, and in revised form, June 6, 2019 Published, Papers in Press, June 14, 2019, DOI 10.1074/jbc.RA118.007185

Flore De Wit[‡], Sambasiva Rao Pillalamarri[§], Alba Sebastián-Martín[‡¶], Akkaladevi Venkatesham[§], Arthur Van Aerschot[§1], and Zeger Debyser[‡2]

From the [‡]Laboratory for Molecular Virology and Gene Therapy, Department of Pharmaceutical and Pharmacological Sciences and the [§]Medicinal Chemistry, Rega Institute for Medical Research, Department of Pharmaceutical and Pharmacological Sciences, KU Leuven, 3000 Leuven, Belgium and the [¶]Centro de Biología Molecular "Severo Ochoa", Consejo Superior de Investigaciones Científicas & Universidad Autónoma de Madrid, 28006 Madrid, Spain

Edited by John M. Denu

Only a small portion of human immunodeficiency virus type 1 (HIV-1) particles entering the host cell results in productive infection, emphasizing the importance of identifying the functional virus population. Because integration of viral DNA (vDNA) is required for productive infection, efficient vDNA detection is crucial. Here, we use click chemistry to label viruses with integrase coupled to eGFP ($HIV_{IN\text{-}eGFP}$) and visualize vDNA. Because click labeling with 5-ethynyl-2′-deoxyuridine is hampered by intense background staining of the host nucleus, we opted for developing HIV-1 reverse transcriptase (RT)-specific 2′-deoxynucleoside analogs that contain a clickable triple bond. We synthesized seven propargylated 2′-deoxynucleosides and tested them for lack of cytotoxicity and viral replication inhibition, RT-specific primer extension and incorporation kinetics *in vitro*, and the capacity to stain HIV-1 DNA. The triphosphate of analog A5 was specifically incorporated by HIV-1 RT, but no vDNA staining was detected during infection. Analog A3 was incorporated *in vitro* by HIV-1 RT and human DNA polymerase γ and did enable specific HIV-1 DNA labeling. Additionally, A3 supported mitochondria-specific DNA labeling, in line with the *in vitro* findings. After obtaining proof-of-principle of RT-specific DNA labeling reported here, further chemical refinement is necessary to develop even more efficient HIV-1 DNA labels without background staining of the nucleus or mitochondria.

After fusion of human immunodeficiency virus type 1 (HIV-1)[3] particles with the host cell, the viral capsid cone is released into the cytoplasm and starts its journey toward the nucleus. During this passage, the viral RNA is reverse transcribed into double-stranded viral DNA (vDNA), which forms together with cellular and viral proteins the preintegration complex. Before entering the nucleus through the nuclear pore complex (1), the preintegration complex must, at least partially, uncoat because the cone exceeds the size of the nuclear pore complex channel (2, 3). The subsequent replication steps are closely intertwined confounding their study. In addition, reverse transcriptase (RT) inaccuracy results in a diverse pool of viruses with varying infectivity. Because the large majority of this HIV-1 pool presumably represents noninfectious particles (4), ensemble analysis will mask the truly infectious population. Hence, studies at a single virus level are required to mark and subsequently characterize the smaller infectious population.

Methods to track HIV-1 particles and label vDNA have been reported before. Single HIV-1 particles can be imaged through (i) the incorporation of the *gfp* gene into the *gag* gene of the HIV-1 genome (5, 6), (ii) Vpr transincorporation of GFP (7, 8) or integrase (IN) coupled to eGFP ($HIV_{IN\text{-}eGFP}$) (9, 10), or (iii) the incorporation of a fluorescently labeled host cell factor like tetrameric cyclophilin A tagged with DsRed (CypA-DsRed) (11, 12) or APOBEC3F (A3F) tagged with YFP (13). All these methods are used to study distinct steps in the early replication cycle, such as uncoating, nuclear import, and the influence of different cellular cofactors. Nevertheless, with these techniques, replication-deficient viruses cannot be discriminated from the replication competent ones. Hence, because the integrated vDNA, determines productive infection in the end, additional detection of HIV-1 DNA, on top of viral protein labeling, is necessary. Various methods of vDNA labeling have been used to study the nuclear location of the provirus. These techniques include single-cell imaging of HIV-1 provirus which is based on the immunolabeling of double-stranded breaks in a reporter construct induced by an exogenous endonuclease (14) and the more classical fluorescence *in situ* hybridization (15). Recently, using a more sensitive fluorescence *in situ* hybridization, namely branched DNA labeling, vDNA was detected in the

This work was supported by KU Leuven Grant C14/17/095, Fonds Wetenschappelijk Onderzoek Grants G0A5316N (to Z. D.), G077814N (to A. V. A.), and 1110218N (to F. D. W.), and Spanish Ministry of Education, Culture and Sport Grant FPU2013/00693 (to A. S.-M.). The authors declare that they have no conflicts of interest with the contents of this article.

This article contains supporting Experimental procedures, Table S1, and Figs. S1–S4.

[1] To whom correspondence may be addressed: Medicinal Chemistry, Rega Institute for Medical Research, Dept. of Pharmaceutical and Pharmacological Sciences, KU Leuven, 3000 Leuven, Belgium. Tel.: 32-16-3-21100; E-mail: arthur.vanaerschot@kuleuven.be.

[2] To whom correspondence may be addressed: Laboratory for Molecular Virology and Gene Therapy, Dept. of Pharmaceutical and Pharmacological Sciences, KU Leuven, 3000 Leuven, Belgium. Tel.: 32-16-3-36332; E-mail: zeger.debyser@kuleuven.be.

[3] The abbreviations used are: HIV-1, human immunodeficiency virus type 1; EdU, 5-ethynyl-2′-deoxyuridine; NRTI, nucleoside reverse transcriptase inhibitor; RT, reverse transcriptase; TP, triphosphate; vDNA, viral DNA; MTT, 3-(4,5-dimethylthiazol-2-yl)-2,5-diphenyltetrazolium bromide; IN, integrase; AX, propargyl-containing 2′-deoxynucleoside; MP, monophosphate; FBS, fetal bovine serum; DAPI, 4′,6′-diamino-2-phenylindole; fLuc, firefly luciferase.

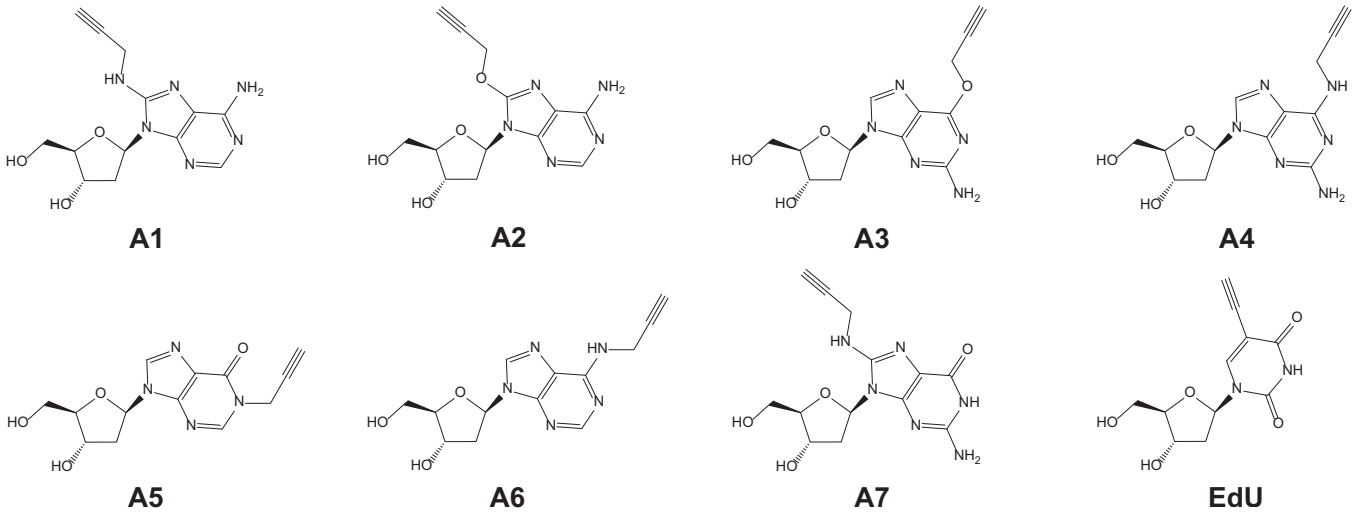

Figure 1. Structures of the modified 2′-deoxynucleosides used in this study. Structures of the propargyl-containing purine 2′-deoxynucleosides (A1 to A7) together with EdU (27) are shown.

cytoplasm and the nucleus (16). This method can also be used to detect viral RNA from incoming particles in the cytoplasm and viral mRNA transcripts (17). Although branched DNA imaging is very sensitive and can be combined with immunolabeling, the reaction conditions abolish eGFP fluorescence used to track viral proteins.

Another elegant DNA-labeling approach is based on the incorporation of 2′-deoxynucleosides containing a triple bond, such as 5-ethynyl-2′-deoxyuridine (EdU) (18, 19). Subsequently, the incorporated nucleosides are visualized through an azide-alkyne cycloaddition with an azide-labeled fluorescent dye (20). In the context of virus labeling, this method was first used to study DNA viruses, like adenovirus, *herpesvirus*, and vaccinia virus, that can be labeled during production (21). Click labeling with EdU has also been used to monitor HIV-1 reverse transcription during the infection of HeLa cells with $HIV_{IN\text{-}eGFP}$ particles (22). In the cytoplasm, EdU-positive IN-eGFP particles were detected, but detection of these spots in the nucleus was hampered by EdU incorporation by the nuclear polymerases. Although Peng *et al.* (22) used the DNA polymerase inhibitor aphidicolin to reduce nuclear incorporation, vDNA detection in the nucleus remained impossible, and mitochondrial DNA labeling increased. Hence, HIV-1 DNA labeling with EdU is more appropriate for nondividing cells with less DNA synthesis like monocyte-derived macrophages (23).

To track HIV-1 DNA synthesis in dividing cells, we attempted to develop virus-specific 2′-deoxynucleosides with a clickable triple bond that are selectively incorporated by HIV-1 RT and not by the cellular DNA polymerases. Although this idea is innovative for virus labeling purposes, the concept of selective RT recognition was used before to develop nucleoside RT inhibitors (NRTIs) (24) and mutagenic nucleosides, which abolish viral replication over multiple rounds (25, 26). To this end, we opted for a series of newly synthesized propargylated 2′-deoxynucleosides (Fig. 1) (27) to achieve selective incorporation into HIV-1 DNA without blocking further DNA synthesis. The ultimate goal of this project is the visualization of single replicating HIV-1 particles based on the combined detection of IN-eGFP and vDNA in the cytoplasm and the nucleus.

Results

Propargylated 2′-deoxynucleosides are less cytotoxic than EdU and do not inhibit HIV-1 replication

Seven propargylated 2′-deoxynucleosides were synthesized as described by Venkatesham *et al.* (27) to obtain specific imaging of HIV-1 DNA based on click chemistry. The propargylated analogs were first evaluated for their cytotoxicity and potential antiviral effect in MT4 cells using the MTT method (28). The analogs displayed no remarkable cell toxicity, whereas the 50% cytotoxic concentration (CC_{50}) value of EdU was lower than the concentration required for efficient labeling (10 μM) (Table 1) (29–31). In the subsequent experiments, the seven analogs were used at a concentration less than or equal to their CC_{50} (Table 1). None of the analogs showed an antiviral effect at concentrations below the cytotoxic concentration.

Propargyl 2′-deoxynucleosides do not inhibit HIV-1 infectivity

To further characterize the impact of the different propargylated 2′-deoxynucleosides on HIV-1 replication, infectivity was examined with a firefly luciferase reporter (HIV-fLuc) and compared with a DMSO control. Overall, the different propargyl-containing analogs did not affect HIV-1 infectivity, except for EdU, which showed a 3-fold inhibition (Fig. 2*A*). Of interest, two of the analogs, A3 and A6, exhibited a 3-fold rise in luciferase activity, reflecting an increased viral infectivity. The addition of the natural 2′-deoxyadenosine in a range of concentrations (0.5–1000 μM) did not affect infectivity to the same extent as analogs A3 and A6 (Fig. 2*B*). Additionally, these two propargylated analogs were also evaluated in a nuclear import assay in which the subcellular localization of fluorescently labeled virus particles ($HIV_{IN\text{-}eGFP}$) is assessed after nuclear lamina staining. The ratio of nuclear IN-eGFP complexes over the total number of complexes was calculated as a measure of nuclear import. No significant differences were detected compared

Table 1
Toxicity and antiviral effect of propargylated 2′-deoxynucleosides in MT4 cells

MT4 cells were incubated with the different 2′-deoxynucleosides in the absence and presence of HIV-1_{IIIB}. The CC_{50} and the EC_{50} of the propargylated analogs and EdU were determined after 5 days with the MTT method. At least two independent experiments were used to calculate the values. If possible, averages and standard deviations were determined. The concentrations used in all cellular experiments are indicated in the right column.

Analog	CC_{50}	EC_{50}	Analog concentration
	μM	μM	μM
EdU	2.2 ± 1.3	>2.2	10
A1	>200	>200	220
A2	>600	>600	620
A3	>600	>600	670
A4	>50	>50	50
A5	>600	>600	660
A6	>1000	>1000	1000
A7	>600	>600	610

with the DMSO control, although a trend toward more nuclear IN-eGFP complexes in the presence of analogs A3 and A6 was observed (Fig. 2*C*). In conclusion, none of the propargylated 2′-deoxynucleosides did inhibit HIV-1 replication, and addition of two analogs, A3 and A6, resulted in an increased infectivity.

Specific incorporation of propargylated 2′-deoxynucleotides

We next analyzed the analog specificity for different polymerases in a primer extension assay, for which we synthesized the respective triphosphates for each analog (AX-TP) (Fig. S1). The incorporation of the propargylated 2′-deoxynucleoside triphosphates by RT, human DNA polymerase α, and human mitochondrial DNA polymerase γ was compared, each tested under optimal reaction conditions. A Cy3-fluorescently labeled 15-mer primer was extended using a 47-mer DNA or RNA template in reaction mixtures where each time one of the natural dNTPs was substituted by a propargylated 2′-deoxynucleotide analog. Because all propargylated analogs are purine-based, no extended bands were observed in the absence of dCTP and dTTP for any polymerase. In contrast, EdU-TP was incorporated by all polymerases instead of dTTP (Fig. 3 and Table S1). For RT, even in conditions lacking dATP a low intensity full-length extension band was detected, reflecting the inaccuracy of the RT. This was observed with both RNA and DNA templates; nevertheless differences in the incorporation efficiency were detected (Fig. 3, *A* and *B*). Using an RNA template, mimicking the first step of reverse transcription (minus-strand DNA synthesis), HIV-1 RT was able to incorporate all analogs except for A1-TP, A2-TP, and A7-TP, achieving a fully extended primer in the absence of dATP (Fig. 3*A*). The intensity of the full-length bands was equal to that in the condition containing the natural dATP for A4-TP and A6-TP and half this intensity for A3-TP and A5-TP (Table 2). A3-TP could also replace dGTP during reverse transcription of the RNA template, yielding ~50% of the full-length primer. Using a DNA template, revealing plus-strand DNA synthesis, HIV-1 RT incorporated A4-TP and A6-TP, reaching ~80% of the full-length extension product compared with in the control condition (Table 2 and Fig. 3*B*). In addition, A3-TP could also be incorporated in the absence of dATP and dGTP but to a smaller extent than the natural triphosphate. On the other hand, human DNA polymerase α exhibited a full-length extension band half as intense as that of natural dATP, when using A4-TP (Table 2), whereas incorporation of A1-TP and A6-TP resulted in some intermediate extension products (Fig. 3*C*). Finally, human mitochondrial DNA polymerase γ incorporated all analogs, except for A5-TP and A7-TP, to the same extent as the natural dATP (Table 2 and Fig. 3*D*). None of the analogs could replace dGTP with either human DNA polymerases. In conclusion, to label the HIV-1 DNA specifically, the propargylated 2′-deoxynucleotide analog ought to be incorporated only by RT and not by the human DNA polymerases. Analog A5-TP is the only analog that fulfils this requirement. Various other analogs, *e.g.* A3-TP, A4-TP, and A6-TP, can also be used by RT but at the same time are recognized by human DNA polymerase α and/or mitochondrial DNA polymerase γ.

Incorporation kinetics of propargylated 2′-deoxynucelotides

To further study the incorporation of the different propargylated 2′-deoxynucleotides by HIV-1 RT, steady-state kinetic parameters were determined and compared with those of the natural dATP. The incorporation of a single nucleotide was examined in the presence of each propargylated 2′-deoxynucleotide analog that showed full-length extension in the primer extension assay. A negative control (A2-TP) and a positive control (the natural dATP) were included, and both DNA and RNA templates were used. With the DNA template, incorporation of analogs A3-TP, A4-TP, and A6-TP was assessed (Fig. 4*A*). The gels were quantified, and the reaction velocities were calculated and plotted in function of the nucleotide concentration (Fig. S2*A*). These data were fitted with a Michaelis–Menten equation using GraphPad Prism, and different parameters were calculated: the K_m, k_{cat}, the catalytic efficiency (k_{cat}/K_m), and the relative efficiency ($(k_{cat}/K_m)_{analog}/(k_{cat}/K_m)_{dATP}$) (Table 3). A similar analysis was done with the RNA template, and analogs A1-TP, A3-TP, A4-TP, A5-TP, and A6-TP (Fig. 4*B*, Fig. S2*B*, and Table 3). Overall, no large differences were observed when using the DNA template, although a lower K_m was found for dATP incorporation compared with the analogs. A4-TP was incorporated 2-fold, A6-TP was incorporated 4-fold, and A3-TP was incorporated 5-fold less efficiently than dATP. When using the RNA template, again a lower K_m was found for dATP incorporation compared with the analogs (Table 3). A1-TP was incorporated 33-fold less efficiently than dATP, resulting in a low k_{cat}, a high K_m, and a low relative efficiency. A4-TP was incorporated 2-fold, A6-TP was incorporated 3-fold, and A3-TP was incorporated 8-fold less efficiently than dATP. In the primer extension experiments, A5-TP was the only analog that was selectively incorporated by HIV-1 RT, in the presence of an RNA template. However, in the steady-state experiments, only a low incorporation efficiency was reached, which could not be fitted with a Michaelis–Menten equation. Neither with the DNA nor the RNA template, was incorporation of A2-TP detected. Overall, analog A4-TP was most efficiently incorporated by HIV-1 RT using a DNA and RNA template, although this analog was also incorporated by human DNA polymerase α and human mitochondrial DNA polymerase γ in the primer extension reactions. Hence, A4 is not a good candidate for HIV-1–specific DNA labeling, and analogs A3-TP and A6-TP, which

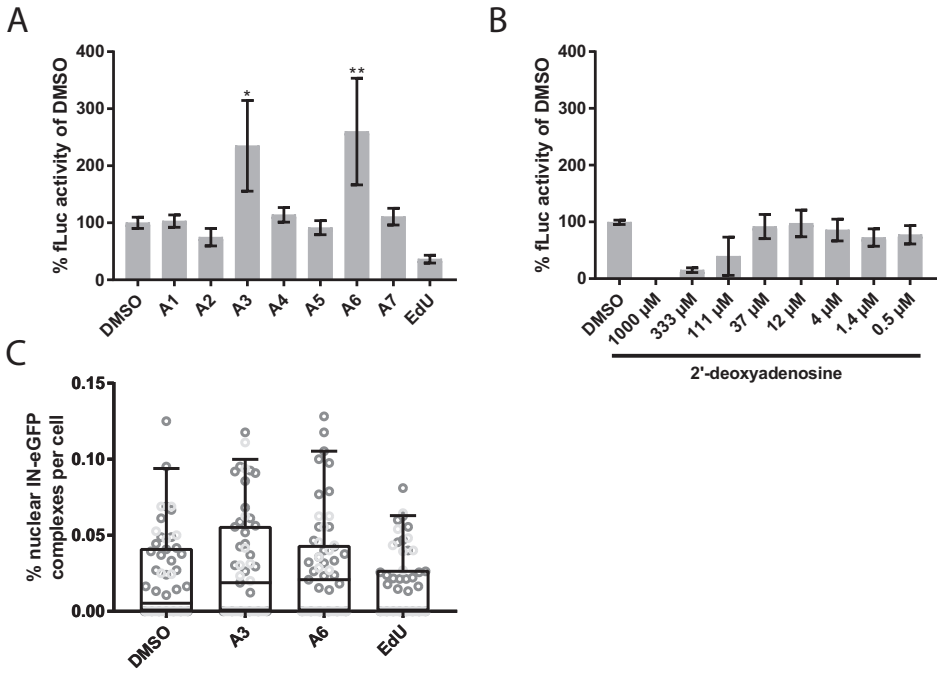

Figure 2. Stimulation of HIV infection in the presence of analogs A3 and A6. HeLaP4 cells were infected in the presence of each propargylated 2′-deoxynucleoside, EdU, or 2′-deoxyadenosine with single-round virus expressing firefly luciferase (*fLuc*; *A* and *B*) or containing eGFP labeled integrase ($HIV_{IN\text{-}eGFP}$; *C*). *A* and *B*, luciferase activity was measured 72 h post-infection. The data from one representative virus dilution are shown in the graph and represented as relative infectivity compared with the DMSO control. The data are means of at least two independent experiments, and the *error bars* represent the standard deviation. A Kruskal–Wallis test was used to test for statistical significance: *, $p < 0.05$; and **, $p < 0.01$. *C*, 6 h post-infection, the cells were fixed, and the percentage of nuclear IN-eGFP complexes was calculated with an in-house MatLab routine. The data of two independent experiments are represented in a scatter plot. No significant differences could be detected with the Mann–Whitney test.

are incorporated 3-fold less efficiently compared with dATP, are used in the further cellular experiments.

Cellular incorporation of the propargylated 2′-deoxynucleosides

Next, the propargylated 2′-deoxynucleosides were used in a cellular context to validate the *in vitro* data of the primer extension assay. HeLaP4 cells were treated for 7 h with the newly synthesized analogs or EdU, after which they were fixed and stained for cytochrome C together with the click reaction. Afterward, the cells were visualized using confocal microscopy. As described before, in the absence of aphidicolin, EdU labeling resulted in a very strong staining of the nuclear DNA (Fig. 5, *top row*) (22). Unlike EdU, the newly synthesized analogs showed no nuclear staining. For some of the analogs, *e.g.* analogs A1, A2, A5, and A7, no cellular DNA staining at all was detected, although analogs A1 and A2 were incorporated *in vitro* by human mitochondrial DNA polymerase γ. Other analogs (*e.g.* A3, A4, and A6) showed some DNA staining after performing the click reaction (Fig. 5). Although all three analogs were incorporated by human mitochondrial DNA polymerase γ in the primer extension assay, only A3 induced a clear mitochondrial staining, as visualized by co-staining with cytochrome C. Analogs A4 and A6 showed a speckled pattern, which was not overlapping with the cytochrome C staining. To validate analog A3 as a mitochondrial DNA marker, various other cell lines (MT4, SupT1, and Jurkat) and primary CD4+ T cells were also subjected to A3 click staining. Co-localization of A3 click staining and cytochrome C could also be detected in these T cells (Fig. S3).

Incorporation of the propargylated 2′-deoxynucleosides during HIV-1 infection

Subsequently, HeLaP4 cells were infected with IN-eGFP fluorescently labeled virus ($HIV_{IN\text{-}eGFP}$) in the presence of the propargylated 2′-deoxynucleosides. The cells were pretreated with the analogs or EdU for 1 h before infection to allow phosphorylation to occur. After 6 h of infection, the cells were fixed, and the click reaction was performed. Stainings were visualized by confocal microscopy. In these images, co-localization between eGFP-labeled IN and click DNA staining was scored. Infection in the presence of EdU resulted in distinct IN-eGFP–positive EdU spots, which were only visible in the cytoplasm because of a high background incorporation in the nucleus by the cellular polymerases (Fig. 6). On average, 4.5% of the IN-eGFP complexes contained also EdU- positive vDNA. For most of the analogs, *e.g.* analogs A1, A2, A5, and A7, no vDNA staining could be detected. With analog A4, click DNA staining was observed in infected and noninfected cells; however, no overlap with IN-eGFP could be detected (data not shown). As in the noninfected cells, a clear mitochondrial staining was detected in the presence of analog A3. In addition, IN-eGFP–positive A3 spots were detected (Fig. 6), although fewer than with EdU. Approximately 1.7% of the IN-eGFP complexes showed A3-based vDNA labeling. Overlap between IN-eGFP and the click DNA staining with analog A6 was observed as well (Fig. 6), but only 0.6% of the IN-eGFP complexes contained a vDNA label. In conclusion, IN-eGFP–positive click spots were detected in the presence of EdU and the newly synthesized analogs A3 and A6.

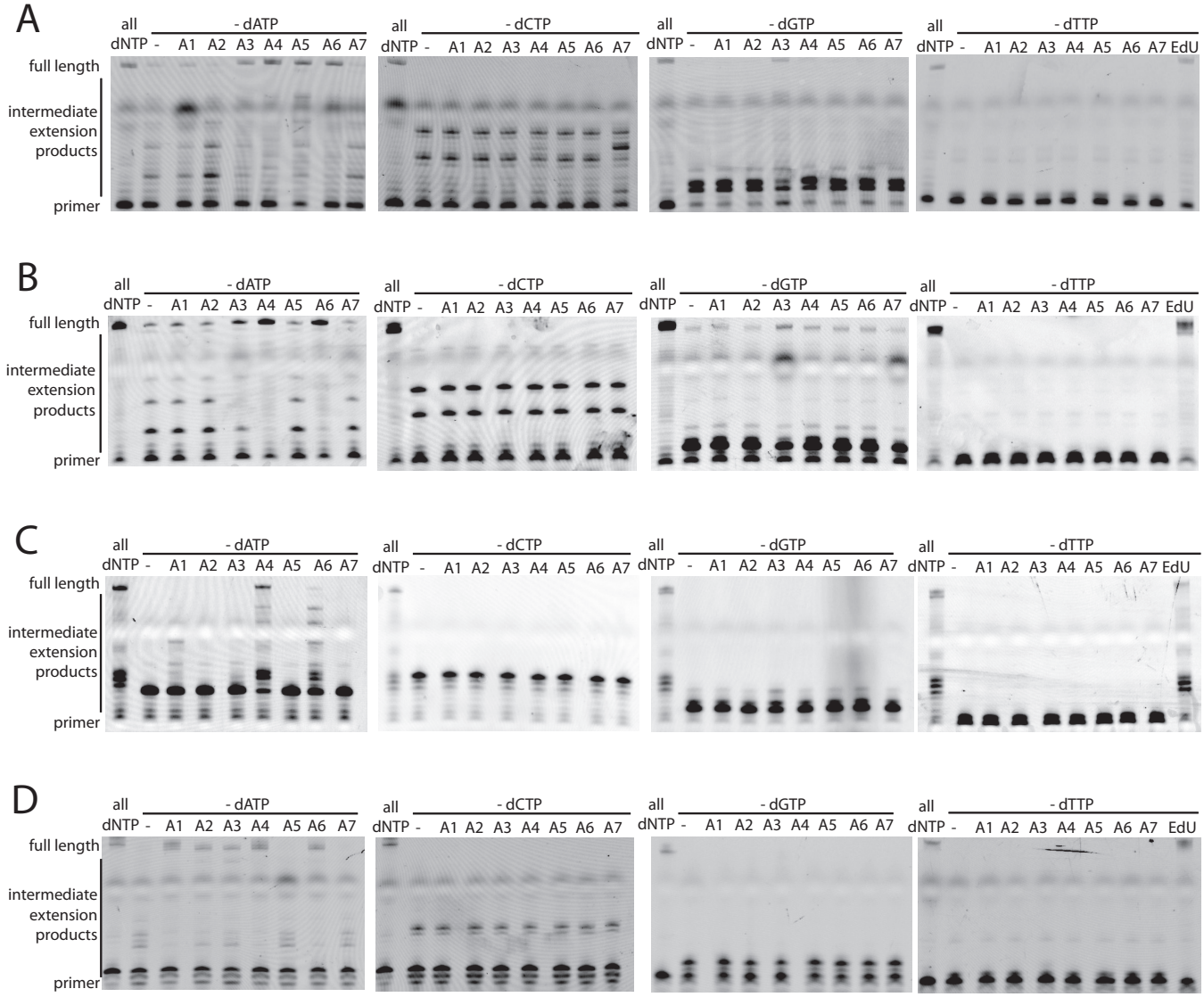

Figure 3. Primer extension by HIV-1 RT and human DNA polymerases α and γ. A Cy3-labeled 15-mer 2′-deoxynucleotide primer was annealed to either a 47-mer RNA template (*A*) or a 47-mer DNA template (*B–D*) and extended by RT (*A* and *B*), human DNA polymerase α (*C*), or human mitochondrial DNA polymerase γ (*D*). Per condition, the four natural dNTPs were substituted by each propargylated nucleoside triphosphate (A1-TP to A7-TP) or EdU-TP. Reactions were carried out for 5 min (RT), 60 min (human DNA polymerase α), or 120 min (human mitochondrial DNA polymerase γ). The reaction products were run on a denaturing polyacrylamide gel and visualized with a Typhoon FMA9500 at 532 nm. The positions of migration of the unextended 15-mer primer and the fully extended 47-mer product are indicated. Representative gels are shown for each condition.

Table 2

Quantification of primer extension data

A Cy3-labeled 15-mer 2′-deoxynucleotide primer was annealed to either a 47-mer RNA template or a 47-mer DNA template and extended by HIV-1 RT, human DNA polymerase α, or human mitochondrial DNA polymerase γ. In each condition, one of the four natural dNTPs was substituted by the propargylated triphosphate analog (A1-TP to A7-TP). The percentage full-length primer extension in presence of the propargyl 2′-deoxynucleoside triphosphate compared with the extension in the presence of the natural dNTP was calculated. The results are the averages of three independent experiments.

Polymerase	Substituted dNTP	-dNTP	A1-TP	A2-TP	A3-TP	A4-TP	A5-TP	A6-TP	A7-TP
		%	%	%	%	%	%	%	%
RT (RNA)	dATP	0	12 ± 12	0	49 ± 12	81 ± 12	42 ± 11	76 ± 20	0
	dGTP	0	0	0	45 ± 20	0	0	0	0
RT (DNA)	dATP	0	4 ± 3	0	20 ± 7	83 ± 23	3 ± 2	78 ± 20	0
	dGTP	0	0	0	25 ± 16	0	0	0	0
Human DNA polymerase α	dATP	0	0	0	0	54 ± 11	0	0	0
Human DNA polymerase γ	dATP	0	97 ± 6	79 ± 30	63 ± 12	106 ± 18	0	111 ± 39	0

To validate the specificity of the vDNA staining, a virus containing a catalytically inactive reverse transcriptase mutant, $RT^{D185N/D186N}$ (see supporting Experimental Procedures), was used. For this mutant, no RT activity was observed in a SYBR Green product-enhanced RT assay (Fig. S4*A*), and no reverse transcripts were detected by quantitative PCR analysis (Fig. S4*B*) (see supporting Experimental Procedures). The cells were infected with a similar amount of WT and mutant virus in the

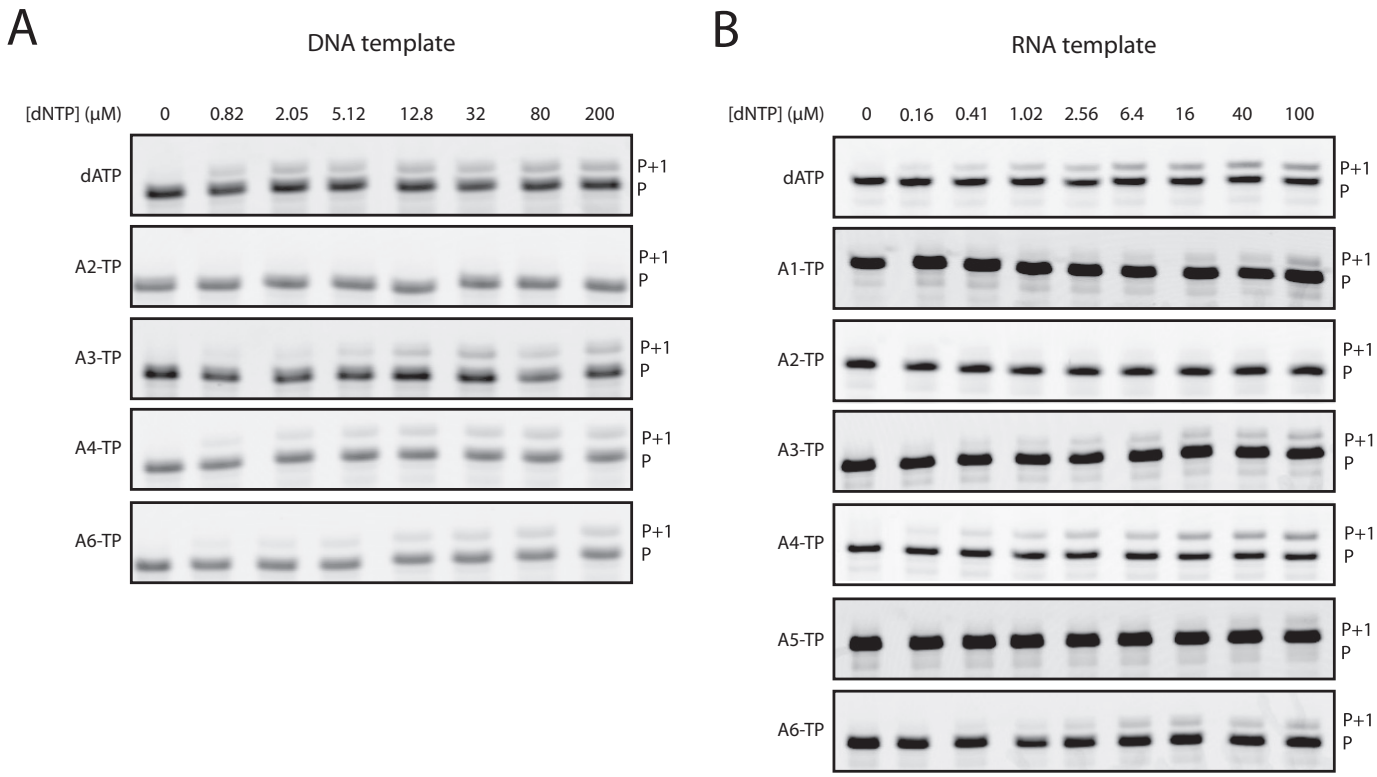

Figure 4. Single-nucleotide incorporation by HIV-1 RT. A Cy3-labeled 15-mer 2′-deoxynucleotide primer was annealed to either a 25-mer DNA template (*A*) or a 25-mer RNA template (*B*). For each propargylated 2′-deoxynucleoside triphosphate showing incorporation in the primer extension reactions, a range of concentrations (0.82–200 μM for the DNA template and 0.16–100 μM for the RNA template) was added to initiate the reaction. A2-TP was included as a negative control, and dATP was included as a positive control. Reactions with the DNA template were carried out for 40 s, and those with the RNA template were carried out for 30 s to 15 min, depending on the substrate. The reaction products were run on a denaturing polyacrylamide gel, and the primer (*P*) and primer that incorporated a single nucleotide ($P + 1$) were visualized with a Typhoon FMA9500 at 532 nm. Representative gels are shown for each condition.

Table 3

Single-nucleotide incorporation kinetics

A Cy3-labeled 15-mer 2′-deoxynucleotide primer was annealed to either a 25-mer RNA template or a 25-mer DNA template, and a single natural nucleotide or analog incorporation by HIV-1 RT was assessed. The reactions were conducted in the initial linear range of product formation and with a large excess of substrate. The reaction velocity was determined in three independent experiments and plotted as a function of the nucleotide concentration, and the single-nucleotide incorporation kinetic parameters were derived by fitting the data to the Michaelis–Menten equation. The catalytic efficiency (k_{cat}/K_m) and relative efficiency ($(k_{cat}/K_m)_{analog}/(k_{cat}/K_m)_{dATP}$) were calculated.

	k_{cat}	K_m	k_{cat}/K_m	Relative efficiency
	min^{-1}	μM	$\mu M^{-1}\ min^{-1}$	
DNA template				
dATP	1.79 ± 0.047	0.82 ± 0.14	2.18	1
A3-TP	1.68 ± 0.081	3.89 ± 0.87	0.43	0.20
A4-TP	1.90 ± 0.051	1.60 ± 0.23	1.19	0.54
A6-TP	1.77 ± 0.064	3.17 ± 0.55	0.56	0.26
RNA template				
dATP	4.03 ± 0.12	1.33 ± 0.19	3.03	1
A1-TP	1.17 ± 0.11	13.65 ± 3.96	0.09	0.03
A3-TP	3.27 ± 0.30	8.22 ± 3.48	0.40	0.13
A4-TP	2.53 ± 0.11	2.02 ± 0.724	1.25	0.41
A6-TP	2.82 ± 0.16	3.24 ± 0.76	0.87	0.29

presence of the analogs and analyzed as previously described. The number of IN-eGFP–positive click spots was compared between both conditions. Infection with virus containing $RT^{D185N/D186N}$ resulted in less EdU co-localizing IN-eGFP spots than with virus containing RT^{WT} (Fig. 7*A*). There was a 3-fold increase in cells showing no co-localization and a 3-fold drop in cells containing two or three co-localizing spots. In the presence of analog A3, the difference with the mutant virus was less clear. Slightly more cells showed no co-localization, and fewer cells showed one co-localizing spot in the presence of the catalytically inactive mutant (Fig. 7*B*). There was no obvious difference between RT^{WT} and $RT^{D185N/D186N}$ for analog A6 (Fig. 7*C*).

Discussion

In this study, we aimed to visualize single RT-competent HIV-1 particles based on the combined detection of IN fused to eGFP ($HIV_{IN\text{-}eGFP}$) and vDNA. The various HIV-1 vDNA labeling methods reported so far visualize integrated provirus (14, 15) or cannot be combined with eGFP fluorescence (16, 17). Hence, we selected a click chemistry method, which is based on the incorporation of ethynyl-modified 2′-deoxynucleosides and the subsequent reaction with an azide-labeled fluorescent dye through the azide-alkyne cycloaddition (20). Click chemistry was already used in combination with eGFP fluorescence to visualize HIV-1 vDNA, by making use of the commercially available EdU, although the detection was only possible in the cytoplasm because of the incorporation of EdU by the nuclear polymerases (22). By using a polymerase inhibitor, aphidicolin, nuclear incorporation was reduced, but in addition mitochondrial staining was increased. For this reason, we aimed to develop virus-specific nucleoside analogs containing a clickable triple bond, which are not recognized by the cellular DNA polymerases but selectively incorporated by RT. Because of the lower fidelity of HIV-1 RT compared with other DNA polymer-

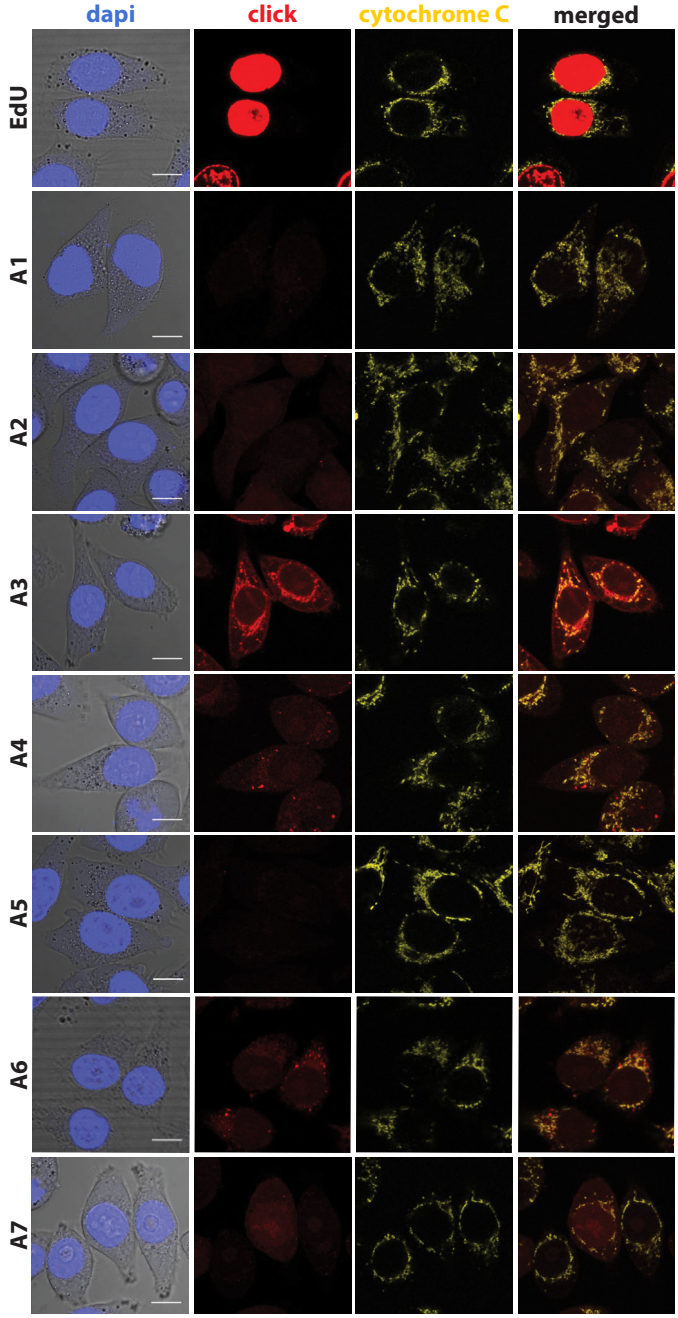

Figure 5. Cellular incorporation of 2′-deoxynucleoside analogs in noninfected cells. HeLaP4 cells were treated with the different analogs or EdU for 7 h. Afterward they were fixed and click stained (*red*) together with a nuclear (DAPI, *blue*) and cytochrome C (*yellow*) staining. Confocal microscopy was used to acquire *Z* stacks covering the whole-cell volume. *Scale bars*, 10 μm.

ases and the lack of proofreading activity (32–34), developing such HIV-1–specific propargylated 2′-deoxynucleosides should be feasible.

In this study, HIV-1–specific nucleoside analogs are for the first time used to selectively label HIV-1 vDNA, although the concept was used before to generate HIV-1 NRTIs, which terminate HIV-1 reverse transcription elongation, as well as mutagenic nucleosides, which abolish viral replication over multiple replication rounds (25, 26). Most DNA polymerases (*e.g.* α, δ, and ϵ) are insensitive to inhibition by HIV-1 NRTIs; however, human mitochondrial DNA polymerase γ poorly discriminates between endogenous dNTPs and nucleoside analogs (35, 36) and has a lower exonuclease activity (37). Therefore, incorporation of the HIV-1–specific propargyl modified 2′-deoxynucleosides by the human mitochondrial polymerase γ needs to be avoided as well.

To achieve selective visualization of HIV-1 vDNA, Venkatesham *et al.* (27) synthesized a series of propargyl-containing 2′-deoxynucleosides (Fig. 1). Initially, the cytotoxicity of the newly synthesized purine 2′-deoxynucleosides was examined, in addition to EdU. Because the analogs were less or not toxic compared with EdU, incorporation by the human DNA polymerases was expected to be lower (Table 1). In single- and multiple-round HIV-1 replication, none of the analogs negatively affected HIV-1 infectivity (Table 1 and Fig. 2*A*). On the other hand, two of the newly synthesized analogs, analogs A3 and A6, could increase luciferase expression, indicating a higher infection capability. Interestingly, this effect was not detected when we provided the virus with increased levels of the natural substrate 2′-deoxyadenosine (Fig. 2*B*). Because analogs A3 and A6 are likely incorporated selectively by RT, our data suggest an increased supply of RT substrate and increased levels of reverse transcription, followed by integration and subsequent firefly luciferase expression. This mechanism, however, still needs to be elucidated.

The selectivity of the analogs was examined *in vitro* with a primer extension assay (Fig. 3), for which we synthesized the corresponding 2′-deoxynucleoside triphosphates of all analogs. Human DNA polymerase α, an essential polymerase for genome replication, was used to study nuclear incorporation, next to human mitochondrial DNA polymerase γ and HIV-1 RT. As the cytotoxicity results already indicated (Table 1), most analogs were not incorporated by human DNA polymerase α. Only analog A4-TP could substitute for dATP (Fig. 3*C* and Table 1). Several analogs were incorporated by HIV-1 RT in the primer extension experiments. Notably, more analogs were incorporated with the RNA template compared with the DNA template (Figs. 3*A* and 3*B*).

The incorporation efficiency of the analogs by HIV-1 RT was further studied with steady-state kinetics (Fig. 4, Table 3, and Fig. S2). These experiments showed that A4 was the analog that was incorporated most efficiently by HIV-1 RT. Like described above, this analog was also used by human DNA polymerase α, which hampers the use of analog A4 as a HIV-1–specific DNA label. Analogs A3 and A6 were also incorporated by HIV-1 RT, although less efficiently than dATP. The analogs were used 5-fold and 4-fold less efficiently using a DNA template and 8-fold and 3-fold less efficiently using an RNA template, for A3-TP and A6-TP, respectively. Because analog A5-TP was the only analog selectively incorporated by HIV-1 RT in the primer extension reactions using an RNA template, it was also examined in the steady-state kinetic reactions. In these reactions, only a faint extended primer band could be detected at longer time points (up to 15 min), and subsequently the kinetic parameters could not be determined. Altogether, different analogs could be incorporated by HIV-1 RT, although the efficiency for the analogs was always lower than for the natural dATP. In these reaction conditions, interestingly, HIV-1 RT seems to

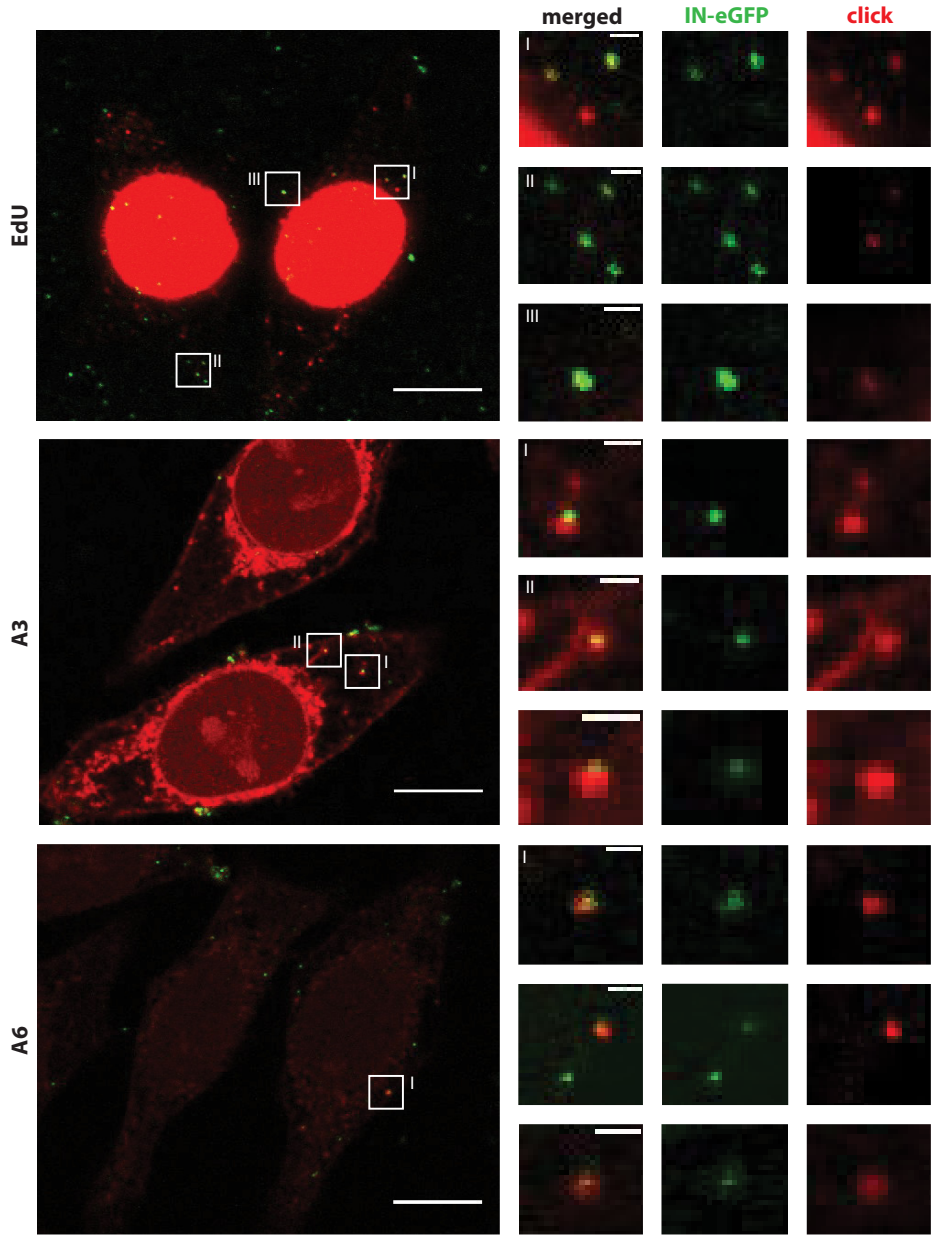

Figure 6. HIV-1 vDNA labeling in HeLaP4 cells. HeLaP4 cells were infected with $HIV_{IN\text{-}eGFP}$ in the presence of the respective analogs and EdU for 6 h, followed by fixation and click labeling. Confocal microscopy was used to acquire *Z* stacks covering the whole-cell volume. Images were analyzed for IN-eGFP (*green*) positive click spots (*red*), representing RT competent viruses. *Scale bars* in overview images, 10 μm. *Scale bars* in magnifications, 1 μm.

have a higher fidelity when using a DNA template compared with an RNA template.

As mentioned above, human mitochondrial DNA polymerase γ does not possess the ability to discriminate between natural dNTPs and analogs and has a lower exonuclease activity, which resulted in a high frequency of analog incorporation in the primer extension assay (Fig. 3*D*). When comparing these results with the cellular click staining, analog A3 resulted in a clear mitochondrial staining, as shown by co-localization with cytochrome C (Fig. 5 and Fig. S3). Although analogs A1, A2, A4, and A6 were incorporated by human mitochondrial DNA polymerase γ *in vitro*, they did not show a mitochondrial pattern in the cellular experiments. To achieve an active triphosphate that can be incorporated by the polymerases in the cell, the propargyl 2′-deoxynucleosides must be phosphorylated by kinases like adenosine phosphotransferase, adenylate, and guanylate kinases (24, 38). The propargyl group on the modified analogs could interfere with the phosphorylation steps and subsequently prevent the compound to be anabolized to the required triphosphate state. This can result in lack of cellular staining and possibly explain the discrepancy between results from *in vitro* and cellular assays. Unexpectedly, analog A3 provided us with a mitochondrial-specific labeling method, which can be exploited in cell biology.

In the imaging experiments where the click reaction was performed in the presence of $HIV_{IN\text{-}eGFP}$, both analogs A3 and A6 resulted in IN-eGFP–positive click spots. In the presence of analog A3, however, the detection of the IN-eGFP–positive

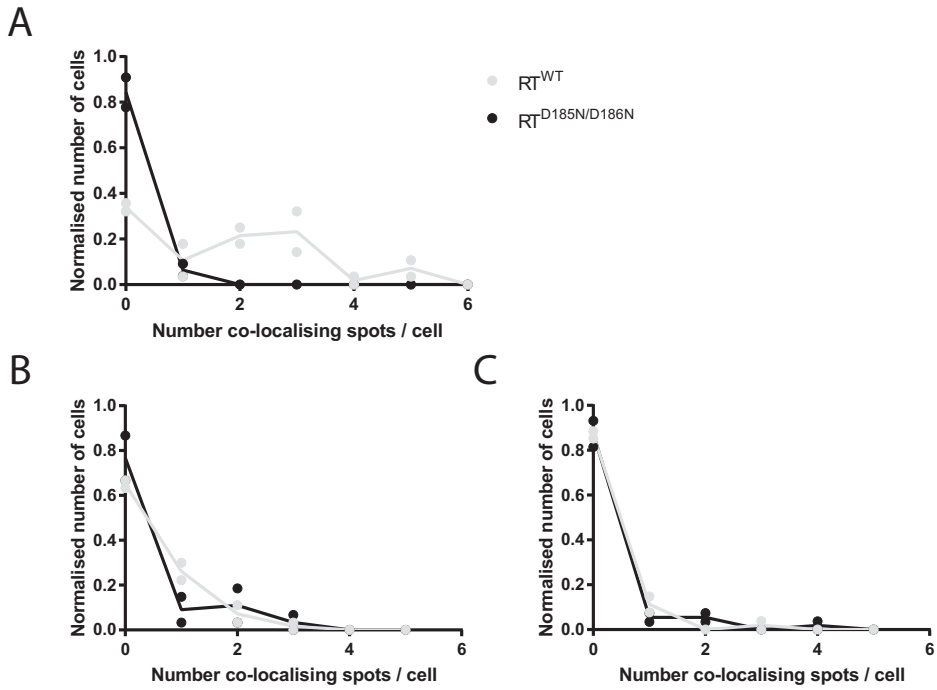

Figure 7. Effect of catalytically inactive reverse transcriptase on HIV-1 vDNA detection. HeLaP4 cells were infected with $HIV_{IN\text{-}eGFP}$ containing RT^{WT} (*gray*) or a catalytically inactive $RT^{D185N/D186N}$ (*black*) in the presence of EdU (*A*), analog A3 (*B*), or analog A6 (*C*) for 6 h, followed by fixation and click labeling. Confocal microscopy was used to acquire *Z* stacks covering the whole-cell volume. Images were analyzed for IN-eGFP–positive click spots, representing RT-competent viruses. The number of cells containing this specific number of click spots, normalized on the total number of cells, was plotted in the graphs. Data from two independent experiments (*circles*) and the mean of both (*lines*) are shown in the graph.

click spots was hampered by the mitochondrial DNA staining (Fig. 6). When using a catalytically inactive RT mutant, the number of co-localizing spots was reduced, but not to the same extent as with the EdU vDNA labeling (Fig. 7, *A* and *B*). When using analog A6, co-localization was only detected with a low frequency, and no reduction was seen with the catalytically inactive RT mutant (Fig. 7*C*). Consequently, we currently cannot assure that the A6 click staining co-localizing with IN-eGFP results from reverse transcription.

Analog A5 is the only propargylated 2′-deoxynucleoside triphosphate that was selectively incorporated by HIV-1 RT based on the primer extension experiments (Fig. 3 and Table 2). Whereas this modification is still accepted by the more forgiving HIV-1 RT, the lack of recognition of A5-TP by other polymerases seems quite plausible in view of the unusual N1-alkylated base. *In vitro*, analog A5 seemed the best candidate for specific HIV-1 vDNA staining, but in the cellular experiments no vDNA staining could be observed. As suggested above for other analogs, a block somewhere in the phosphorylation pathway can hamper incorporation in the cell. The synthesis of a phosphorylated prodrug of analog A5 could circumvent this problem and in the end result in a specific HIV-1 vDNA labeling. The latter, however, is not straightforward in view of the remaining 3′-secondary alcohol.

In conclusion, although the O^6-propargyl-dG (A3) (27) provides clear mitochondrial staining, the sensitivity to detect vDNA in single HIV-1 particles is low, probably because of poor incorporation or phosphorylation defects in the cell. Nevertheless, our rationale seems successful and our limited structure–activity relationship provides input for further chemical synthesis to finally develop an HIV-1 vDNA labeling based on click chemistry without background staining of the nucleus or mitochondria.

Experimental procedures

General procedure for the synthesis of propargyl-containing 2′-deoxynucleoside triphosphates (AX-TP) and monophosphates (AX-MP)

To a stirred solution of propargyl-containing 2′-deoxynucleoside (10 mg, 0.03 mmol, AX) in 100 μl of trimethylphosphate at −5 °C, phosphorous oxychloride (0.09 mmol) was added, and the mixture was stirred for 60 min. After completion of the reaction monitored by TLC (mobile phase: isopropanol: water:aqueous (aq). ammonia, 7:2:1), a prechilled mixture containing tris-tetrabutyl-ammonium hydrogen pyrophosphate (0.15 mmol) and 400 μl of anhydrous dimethylformamide (DMF) were added to the reaction mixture over a period of 10 min followed by 40 μl of tributyl amine and kept under stirring for 10 min. The reaction mixture was quenched by slow addition of 1 ml of TEAB buffer and was stirred further for 10 min. The total reaction mixture was lyophilized, and the obtained crude material subjected to HPLC chromatography using a Mono-Q ionic exchange column (GE Healthcare Life Sciences), which was eluted using a linear gradient from 0.025 to 1 M TEAB. The fractions containing the desired product were pooled, evaporated, and co-evaporated with water (3 × 5 ml) obtaining the pure propargyl-containing 2′-deoxynucleoside triphosphates (AX-TP, Fig. S1). The method also allowed isolation of the respective monophosphate intermediates (AX-

MP). The extinction coefficient (ϵ-values) as determined at 260 nm for the respective nucleosides was used to determine the isolated amounts and concentrations for the incorporation assays.

((2R, 3S, 5R)-5-(6-amino-8-(prop-2-yn-1-ylamino)-9H-purin-9-yl)-3-hydroxytetrahydrofuran-2-yl)methyl tetrahydrogen triphosphate (A1-TP)

^{31}P NMR (D_2O, 300 MHz): δ −10.75 (d, J = 19.3 Hz, 1P), −11.82 (d, J = 19.3 Hz, 1P), −23.21 (t, J = 19.3 Hz, 1P); UV λ_{max} (nm): 276 (ϵ_{260} 9,200); HR-ESI MS (*m/z*): calculated for $C_{13}H_{19}N_6O_{12}P_3$ [M-H]$^-$: 543.0201; found 543.0208.

((2R, 3S, 5R)-5-(6-amino-8-(prop-2-yn-1-yloxy)-9H-purin-9-yl)-3-hydroxytetrahydrofuran-2-yl)methyl tetrahydrogen triphosphate (A2-TP)

^{31}P NMR (D_2O, 300 MHz): δ −6.54 (d, J = 20.8 Hz, 1P), −11.15 (d, J = 19.3 Hz, 1P), −22.60 (t, J = 20.8 Hz, 1P); UV λ_{max} (nm): 260 (ϵ_{260} 13,875); HR-ESI MS (*m/z*): calculated for $C_{13}H_{18}N_5O_{13}P_3$ [M-H]$^-$, 544.0042; found 544.0041.

((2R, 3S, 5R)-5-(2-amino-6-(prop-2-yn-1-yloxy)-9H-purin-9-yl)-3-hydroxytetrahydrofuran-2-yl)methyl tetrahydrogen triphosphate (A3-TP)

^{31}P NMR (D_2O, 300 MHz): δ −10.87 (d, J = 20.8 Hz, 1P), −11.39 (d, J = 19.3 Hz, 1P), −23.19 (t, J = 19.3 Hz, 1P); UV λ_{max} (nm): 282, 245 (ϵ_{260} 4,200); HR-ESI MS (*m/z*): calculated for $C_{13}H_{18}N_5O_{13}P_3$ [M-H]$^-$, 544.0411; found 544.0043.

((2R, 3S, 5R)-5-(2-amino-6-(prop-2-yn-1-ylamino)-9H-purin-9-yl)-3-hydroxytetrahydrofuran-2-yl)methyl tetrahydrogen triphosphate (A4-TP)

^{31}P NMR (D_2O, 300 MHz): δ −7.49 (d, J = 20.8 Hz, 1P), −12.21 (d, J = 19.3 Hz, 1P), −23.38 (t, J = 20.8 Hz, 1P); UV λ_{max} (nm): 282, 259 (ϵ_{260} 8,830); HR-ESI MS (*m/z*): calculated for $C_{13}H_{19}N_6O_{12}P_3$ [M-H]$^-$, 543.0201; found 543.0202.

((2R, 3S, 5R)-3-hydroxy-5-(6-oxo-1-(prop-2-yn-1-yl)-9H-purin-9-yl)THF-2-yl)methyl tetra-hydrogen triphosphate (A5-TP)

^{31}P NMR (D_2O, 300 MHz): δ −10.83 (d, J = 20.8 Hz, 1P), −11.39 (d, J = 20.8 Hz, 1P), −23.28 (t, J = 19.3 Hz, 1P); UV λ_{max} (nm): 250 (ϵ_{260} 6,525); HR-ESI MS (*m/z*): calculated for $C_{13}H_{17}N_4O_{13}P_3$ [M-H]$^-$, 528.9932; found 528.9944.

((2R, 3S, 5R)-3-hydroxy-5-(6-(prop-2-yn-1-ylamino)-9H-purin-9-yl)THF-2-yl)methyl tetrahydrogen triphosphate (A6-TP)

^{31}P NMR (D_2O, 300 MHz): δ −10.72 (d, J = 19.3 Hz, 1P), −11.29 (d, J = 19.3 Hz, 1P), −23.3 (t, J = 21.7 Hz, 1P); UV λ_{max} (nm): 265 (ϵ_{260} 16,350); HR-ESI MS (*m/z*): calculated for $C_{13}H_{18}N_5O_{12}P_3$ [M-H]$^-$, 528.0091; found 528.0084.

((2R, 3S, 5R)-5-(2-amino-6-oxo-8-(prop-2-yn-1-ylamino)-1,6-dihydro-9H-purin-9-yl)-3-hydroxytetra-hydrofuran-2-yl)methyl tetrahydrogen triphosphate (A7-TP)

^{31}P NMR (D_2O, 300 MHz): δ −10.72 (d, J = 20.8 Hz, 1P), −11.29 (d, J = 19.3 Hz, 1P), −23.59 (t, J = 19.3 Hz, 1P); UV λ_{max} (nm): 259 (br, ϵ_{260} 16,950); HR-ESI MS (*m/z*): calculated for $C_{13}H_{19}N_6O_{13}P_3$ [M-H]$^-$, 559.0150; found 559.0157.

Compounds

EdU (Life Technologies) was dissolved in DMSO at a concentration of 10 mM, and EdU triphosphate (EdU-TP, Jena Bioscience) was dissolved in distilled water at a concentration of 1 mM. The propargyl-containing 2′-deoxynucleosides were synthesized as described by Venkatesham *et al.* (27). All compounds (A1 to A7) were purified on silica gel, and their structures were unambiguously proven by high resolution mass spectrometry (HRMS), UV, ^{1}H NMR, and ^{13}C NMR analysis. The respective triphosphate analogs (AX-TP) were synthesized *via* the method of Ludwig (39) (Fig. S1). The triphosphates were isolated by HPLC (along with the respective monophosphates, AX-MP), and ^{31}P NMR and HRMS analysis corroborated their structure. All propargyl-containing 2′-deoxynucleosides were dissolved in DMSO at a concentration of 100 mM, and the propargylated 2′-deoxynucleoside triphosphates were dissolved in distilled water at a concentration of 1 mM.

Cells

MT4, SupT1, and Jurkat cells were obtained through the National Institutes of Health AIDS Reagent Program, Division of AIDS, NIAID, National Institutes of Health contributed by Dr. D. Richman, Dr. D. Ablashi, and Dr. A. Weiss, respectively. These cells were grown in RPMI 1640 medium (Life Technologies) supplemented with 10% (v/v) fetal bovine serum (FBS, Life Technologies) and 50 μg/ml gentamicin (Life Technologies). HEK-293T (ATCC) cells were cultured in Dulbecco's modified Eagle's medium with GlutaMAX (Life Technologies) supplemented with 5% (v/v) FBS and 50 μg/ml gentamicin. For HeLaP4 cells, a kind gift from Dr. P. Charneau (Institut Pasteur), the previous medium was supplemented with 500 μg/ml Geneticin (Life Technologies). All mammalian cell lines were cultured at 37 °C in a humidified atmosphere with 5% CO_2.

Human peripheral blood mononuclear cells were purified from buffy coats using Lymphoprep following the manufacturer's protocol (Axis-Shield PoC AS). Peripheral blood mononuclear cells were enriched for CD4+ T cells using an anti-human CD3:8 bispecific mAb (0.5 μg/ml, obtained through the National Institutes of Health AIDS Reagent Program, Division of AIDS, NIAID, National Institutes of Health contributed by Drs. J. Wong and G. Alter) during 5 days in RPMI supplemented with human IL2 (100 units/ml, PeproTech), minimal essential medium nonessential amino acids (1×) (Life Technologies) and 15% FBS (Life Technologies). The cells were cultured at 37 °C in a humidified atmosphere with 5% CO_2.

Cell viability assay

3×10^4 MT4 cells were seeded per well in a 96-well plate. To define the CC_{50}, the cells were incubated with a one in three dilution series of the propargylated 2′-deoxynucleosides. To determine the concentration achieving 50% protection against HIV-1 infection, the 50% effective concentration (EC_{50}), cells were preincubated with a one in three dilution series of the nucleoside analogs for 1 h, before they were infected with HIV-1_{IIIB} virus (multiplicity of infection 0.1) together with the respective analogs. Five days after incubation and infection, the viability was examined with the MTT method (42). Briefly, 20 μl of a freshly prepared MTT solution (7.5 mg/ml in PBS,

Sigma–Aldrich) was added to each well to a final volume of 220 μl. After 1 h of incubation at 37 °C, the medium was carefully removed, and the purple formazan crystals were solubilized by adding 10% (v/v) Triton X-100 in acidified isopropanol (0.4% (v/v) methanesulfonic acid, Sigma–Aldrich). The *A* was measured at 540 nm with an EnVision 2130 multilabel plate reader (PerkinElmer). The data were calculated using at least two independent experiments.

Virus production

Vesicular stomatitis virus glycoprotein (VSV-G) pseudotyped single-round HIV-1 particles containing eGFP labeled IN ($HIV_{IN\text{-}eGFP}$) were produced like previously described (9, 10). In short, HEK-293T cells were transfected with 5 μg of pVSV-G, 15 μg of Vpr-IN-eGFP, and 15 μg of pNL4–3.Luc.R^-.E^- containing RT^{WT} or $RT^{D185N/D186N}$ using branched polyethylenimine (10 μM, Sigma–Aldrich). Supernatant was collected 48 h post-transfection, filtered through a 0.45-μm pore-size filter (Sartorius), and concentrated by ultracentrifugation, 90 min at 141,000 × *g* in a SW28 rotor (Beckman Coulter) on a 60% (w/v) iodixanol cushion (Sigma–Aldrich). Afterward, the iodixanol was removed by ultrafiltration (Vivaspin, MWCO 50K, Sartorius). VSV-G pseudotyped HIV-1 particles containing only a firefly luciferase reporter (HIV-fLuc) were produced by transfecting HEK-293T cells with 5 μg of pVSV-G and 15 μg of pNL4–3.Luc.R^-.E^-. Supernatant was collected 48 h post-transfection, filtered through a 0.45-μm pore-size filter, and concentrated by ultrafiltration. Virus was quantified by measuring HIV-1 capsid protein (p24) using a p24 ELISA (INNOTEST p24-ELISA, Innogenetics) following the manufacturer's instructions.

Single-cycle viral infectivity assay

To determine the viral infectivity, 1.5×10^4 HeLaP4 cells were seeded per well in a 96-well plate. The next day, the cells were preincubated with the respective modified 2′-deoxynucleosides (Table 1), the natural 2′-deoxyadenosine in a range of concentrations (0.5–1000 μM) or DMSO for 1 h, before they were infected with a 3-fold dilution of a single-round HIV-fLuc (40, 41) together with the analogs. At 72 h post-infection, the cells were lysed in buffer (50 mM Tris, 200 mM NaCl, 0.2% (v/v) Nonidet P-40, and 5% (v/v) glycerol) and analyzed for firefly luciferase activity (ONE-Glo™; Promega GMBH, Mannheim, Germany). Chemiluminescence was measured with a Glomax luminometer (Promega). Readouts were normalized for protein content as determined by a BCA assay (BCA protein assay kit; Thermo Fisher Scientific). The data are represented as relative infectivity compared with the DMSO control and are means of at least two independent experiments. A Kruskal–Wallis test was used to evaluate statistical significance: *, $p < 0.05$; and **, $p < 0.01$. *Error bars* represent the standard deviation.

Infection and immunolabeling

3×10^4 HeLaP4 cells were seeded per well in poly-D-lysine (Sigma–Aldrich)–coated 8-well chambered coverglasses (Nunc Lab-Tek chambered coverglasses, Thermo Fisher Scientific). The next day, the cells were preincubated for 1 h with the respective modified 2′-deoxynucleosides (Table 1), before they were infected with 1 μg of p24 antigen of $HIV_{IN\text{-}eGFP}$ RT^{WT} or $HIV_{IN\text{-}eGFP}$ $RT^{D185N/D186N}$ together with the analogs. 6 h post-infection, the cells were incubated for 30 s with trypsin (0.25% (w/v), Life Technologies), washed with PBS, fixed for 30 min with 3% (v/v) paraformaldehyde (Sigma–Aldrich), and permeabilized during 20 min with 0.2% (v/v) Triton-X100. Next, nuclei of cells were immunostained with lamin A/C antibody (mouse monoclonal, 1/500 dilution, sc-7292, Santa Cruz Biotechnology) and secondary anti-mouse IgG (H+L) Alexa Fluor 555 conjugate (goat polyclonal, 1/1000 dilution, Thermo Fisher Scientific), or DAPI (1/1000 dilution, Invitrogen) diluted in blocking buffer (1% (w/v) BSA and 0.1% (v/v) Tween 20 in PBS).

For click vDNA labeling, the samples were blocked overnight with PBS containing 3% (w/v) BSA after cell permeabilization with 0.2% (v/v) Triton-X100. The next day, the click reaction was performed following the manufacturer's instructions (Click-iT EdU Alexa Fluor 647 imaging kit, Thermo Fisher Scientific), and the nuclear lamina was immunolabeled as described above. This labeling was also combined with a mitochondrial staining with cytochrome C antibody (mouse monoclonal, 1/400 dilution, 556432, BD Biosciences) and secondary anti-mouse IgG (H+L) Alexa Fluor 555 conjugate (goat polyclonal, 1/1000 dilution, Thermo Fisher Scientific).

6×10^5 MT4, SupT1, Jurkat and CD4+ T cells were seeded per well in poly-D-lysine (Sigma–Aldrich)–coated 8-well chambered coverglasses in the presence of analog A3. 7 h post-infection, the cells were fixed, permeabilized, and stained like described above.

Imaging of the cells was performed using a laser scanning microscope (Fluoview FV1000, Olympus, Tokyo, Japan) with a 60× water objective (NA 1.2), using a 405-nm laser for DAPI excitation, a 488-nm laser for eGFP excitation, a 555-nm laser for Alexa Fluor 555 excitation, and a 635-nm laser for Alexa Fluor 647 excitation. Emission light was collected at 430–470, 505–540, 575–675, and 655–755 nm, respectively. 3D confocal stacks of fixed cells were acquired using a z-step size of 0.3 μm and a sampling speed of 4 μs/pixel. The image resolution was 512 × 512 pixels, a 4× optical zoom, and a pixel size of 103 nm. An in-house MatLab routine (MatWorks) was used to determine the localization and number of IN-eGFP complexes (10). The IN-eGFP complexes were divided into cytoplasmic or nuclear compartments, and the percentage of nuclear IN-eGFP complexes was calculated. Typically, data were collected from at least 25 individual cells. The data of two independent experiments were plotted in a scatter plot, and a Mann–Whitney test was used to determine statistical significance. Co-localization between IN-eGFP and the click DNA staining was determined manually, and the numbers were normalized on the amount of cells measured in each condition. The normalized numbers of two independent experiments were plotted in the graphs.

Primer extension assay

Primer extension reactions were carried out with recombinant HIV-1 RT, human DNA polymerase α, and human mitochondrial DNA polymerase γ. RT was kindly provided by Dr. S. Le Grice and Dr. J. T. Miller (National Cancer Institute, Frederick, MD) and obtained through the National Institutes of Health AIDS Reagent Program, Division of AIDS, NIAID,

National Institutes of Health: HIV-1 RT catalog no. 3555 from Dr. S. Le Grice and Dr. J. T. Miller, human DNA polymerase α was purchased from CHIMERx and human mitochondrial DNA polymerase γ was kindly provided by Dr. M. Falkenberg (University of Gothenburg, Sweden). A fluorescently Cy3-labeled 15-mer DNA primer (5′-AGCTTACGCGCCGAA-3′) was annealed to a 47-mer DNA template (5′-GCTAGACTGAGCTGAACTAGGCTAGACTCCAATTCGGCGCGTAAGCT-3′) or a 47-mer RNA template (5′-GCUAGACUGAGCUGAACUAGGCUAGACUCCAAUUCGGCGCGUAAGCU-3′). The primer/template duplex (2 μM) was prepared by heating a 1:2 mixture of primer and template for 5 min at 95 °C for the DNA template or 90 min at 55 °C for the RNA template and cooling it slowly to room temperature. The reaction mixtures contained 60 mM Tris-HCl buffer (pH 8), 5 mM magnesium acetate, 1 mM DTT, 0.01% (w/v) BSA, 0.1 mM spermine (Sigma–Aldrich), and 200 nM primer/template. Additionally, 2 pmol of RT, 2 units of human DNA polymerase α, or 0.4 pmol of human mitochondrial DNA polymerase γ was supplied. After preincubating the samples for 5 min at 37 °C, the reactions were initiated by the addition of different dNTP mixtures: (i) reactions were all natural dNTPs (250 μM, Thermo Fisher Scientific) were present, (ii) reactions where one of the natural dNTPs was not present, and (iii) reactions where one of the natural dNTPs was not present but with the addition of 40 μM of the modified 2′-deoxynucleoside triphosphate. The reactions were carried out at 37 °C for 5 min (RT), 60 min (human DNA polymerase α), or 120 min (human mitochondrial DNA polymerase γ). At appropriate times, the reactions were quenched by adding stop solution (95% formamide containing 20 mM EDTA, 0.9 mg/ml bromphenol blue, 0.9 mg/ml xylene cyanol, and 0.2% (w/v) SDS). The DNA products were resolved on a denaturing polyacrylamide gel (15% polyacrylamide and 7 M urea) and scanned with a Typhoon FLA9500 (GE Healthcare) at 532 nm. The gels were analyzed using the ImageQuant software (GE Healthcare), and the percentage of full-length extension in the presence of the analogs compared with that with the natural dNTP of three independent experiments was calculated.

Single-nucleotide incorporation kinetics

Steady-state kinetic experiments were carried out with HIV-1 RT. Reaction conditions were identical to the primer extension assay, unless stated otherwise. The same Cy3-labeled primer was used as in the primer extension assay, which was annealed to a 25-mer DNA template (5′-GTCGATCGTTTCGGCGCGTAAGCT-3′) or a 25-mer RNA template (5′-GUCGAUCGUUUCGGCGCGUAAGCU-3′). Reactions were initiated by addition of dATP or modified 2′-deoxynucleoside triphosphate at varying concentrations. Reaction conditions were chosen in the initial linear range of product formation and in the presence of a large excess of substrate. Reactions with the DNA template were carried out for 40 s and with the RNA template for 30 s to 15 min, depending on the substrate (A1, 1 min; A2, 15 min; A3, 30 s; A4, 1 min; A5, 15 min; and A6, 40 s). The DNA products were resolved on a denaturing polyacrylamide gel (20% polyacrylamide and 7 M urea) and scanned with a Typhoon FLA9500 (GE Healthcare) at 532 nm. Gels were analyzed using the ImageQuant software (GE Healthcare). The reaction velocity of three independent experiments was plotted as a function of the nucleotide concentration, and the single-nucleotide incorporation kinetic parameters were derived by fitting the data to the Michaelis–Menten equation. The catalytic efficiency (k_{cat}/K_m) and the relative efficiency ($(k_{cat}/K_m)_{analog}/(k_{cat}/K_m)_{dATP}$) were also calculated.

Author contributions—F. D. W., S. R. P., and A. V. validation; F. D. W., S. R. P., A. S.-M., and A. V. investigation; F. D. W., S. R. P., A. S.-M., and A. V. methodology; F. D. W. writing-original draft; A. V. A. and Z. D. conceptualization; A. V. A. and Z. D. supervision; A. V. A. and Z. D. writing-review and editing; Z. D. and A. V. A. funding acquisition.

Acknowledgments—We thank Paulien Van de Velde, Nam Joo Van der Veeken, Barbara Van Remoortel, and Hoai Nguyen for excellent technical support; Dr. Maria Falkenberg (University of Gothenburg, Gothenburg, Sweden) for the recombinant human mitochondrial DNA polymerase γ; and Dr. Stuart Le Grice and Dr. Jennifer T. Miller (National Cancer Institute, Frederick, MD) for the recombinant HIV-1 reverse transcriptase.

References

1. Suzuki, Y., and Craigie, R. (2007) The road to chromatin: nuclear entry of retroviruses. *Nat. Rev. Microbiol.* **5,** 187–196 CrossRef Medline
2. Ambrose, Z., and Aiken, C. (2014) HIV-1 uncoating: connection to nuclear entry and regulation by host proteins. *Virology* **454-455,** 371–379 CrossRef Medline
3. Campbell, E. M., and Hope, T. J. (2015) HIV-1 capsid: The multifaceted key player in HIV-1 infection. *Nat. Rev. Microbiol.* **13,** 471–483 CrossRef Medline
4. Thomas, J. A., Ott, D. E., and Gorelick, R. J. (2007) Efficiency of human immunodeficiency virus type 1 postentry infection processes: evidence against disproportionate numbers of defective virions. *J. Virol.* **81,** 4367–4370 CrossRef Medline
5. Hübner, W., Chen, P., Del Portillo, A., Liu, Y., Gordon, R. E., and Chen, B. K. (2007) Sequence of human immunodeficiency virus type 1 (HIV-1) Gag localization and oligomerization monitored with live confocal imaging of a replication-competent, fluorescently tagged HIV-1. *J. Virol.* **81,** 12596–12607 CrossRef Medline
6. Mamede, J. I., Cianci, G. C., Anderson, M. R., and Hope, T. J. (2017) Early cytoplasmic uncoating is associated with infectivity of HIV-1. *Proc. Natl. Acad. Sci. U.S.A.* **114,** E7169–E7178 CrossRef Medline
7. McDonald, D., Vodicka, M. A., Lucero, G., Svitkina, T. M., Borisy, G. G., Emerman, M., and Hope, T. J. (2002) Visualization of the intracellular behavior of HIV in living cells. *J. Cell Biol.* **159,** 441–452 CrossRef Medline
8. Campbell, E. M., Perez, O., Melar, M., and Hope, T. J. (2007) Labeling HIV-1 virions with two fluorescent proteins allows identification of virions that have productively entered the target cell. *Virology* **360,** 286–293 CrossRef Medline
9. Albanese, A., Arosio, D., Terreni, M., and Cereseto, A. (2008) HIV-1 pre-integration complexes selectively target decondensed chromatin in the nuclear periphery. *PLoS One* **3,** e2413 CrossRef Medline
10. Borrenberghs, D., Dirix, L., De Wit, F., Rocha, S., Blokken, J., De Houwer, S., Gijsbers, R., Christ, F., Hofkens, J., Hendrix, J., and Debyser, Z. (2016) Dynamic oligomerization of integrase orchestrates HIV nuclear entry. *Sci. Rep.* **6,** 36485 CrossRef Medline
11. Francis, A. C., Marin, M., Shi, J., Aiken, C., and Melikyan, G. B. (2016) Time-resolved imaging of single HIV-1 uncoating *in vitro* and in living cells. *PLoS Pathog.* **12,** e1005709 CrossRef Medline
12. Francis, A. C., and Melikyan, G. B. (2018) Single HIV-1 imaging reveals progression of infection through CA-dependent steps of docking at the

nuclear pore, uncoating, and nuclear transport. *Cell Host Microbe.* **23,** 536–548.e6 CrossRef Medline
13. Burdick, R. C., Hu, W.-S., and Pathak, V. K. (2013) Nuclear import of APOBEC3F-labeled HIV-1 preintegration complexes. *Proc. Natl. Acad. Sci. U.S.A.* **110,** E4780–E4789 CrossRef Medline
14. Di Primio, C., Quercioli, V., Allouch, A., Gijsbers, R., Christ, F., Debyser, Z., Arosio, D., and Cereseto, A. (2013) Single-cell imaging of HIV-1 provirus (SCIP). *Proc. Natl. Acad. Sci. U.S.A.* **110,** 5636–5641 CrossRef Medline
15. Marini, B., Kertesz-Farkas, A., Ali, H., Lucic, B., Lisek, K., Manganaro, L., Pongor, S., Luzzati, R., Recchia, A., Mavilio, F., Giacca, M., and Lusic, M. (2015) Nuclear architecture dictates HIV-1 integration site selection. *Nature* **521,** 227–231 CrossRef Medline
16. Chin, C. R., Perreira, J. M., Savidis, G., Portmann, J. M., Aker, A. M., Feeley, E. M., Smith, M. C., and Brass, A. L. (2015) Direct visualization of HIV-1 replication intermediates shows that capsid and CPSF6 modulate HIV-1 intra-nuclear invasion and integration. *Cell Rep.* **13,** 1717–1731 CrossRef Medline
17. Puray-Chavez, M., Tedbury, P. R., Huber, A. D., Ukah, O. B., Yapo, V., Liu, D., Ji, J., Wolf, J. J., Engelman, A. N., and Sarafianos, S. G. (2017) Multiplex single-cell visualization of nucleic acids and protein during HIV infection. *Nat. Commun.* **8,** 1882 CrossRefMedline
18. Gierlich, J., Burley, G. A., Gramlich, P. M., Hammond, D. M., and Carell, T. (2006) Click chemistry as a reliable method for the high-density functionalisation of alkyne-modified oligodeoxyribonucleotides. *Org. Lett.* **8,** 3639–3642 CrossRef Medline
19. Gierlich, J., Gutsmiedl, K., Gramlich, P. M., Schmidt, A., Burley, G. A., and Carell, T. (2007) Synthesis of highly modified DNA by a combination of PCR with alkyne-bearing triphosphates and click chemistry. *Chemistry* **13,** 9486–9494 CrossRef Medline
20. Salic, A., and Mitchison, T. J. (2008) A chemical method for fast and sensitive detection of DNA synthesis *in vivo*. *Proc. Natl. Acad. Sci. U.S.A.* **105,** 2415–2420 CrossRef Medline
21. Wang, I. H., Suomalainen, M., Andriasyan, V., Kilcher, S., Mercer, J., Neef, A., Luedtke, N. W., and Greber, U. F. (2013) Resource tracking viral genomes in host cells at single-molecule resolution. *Cell Host Microbe* **14,** 468–480 CrossRef Medline
22. Peng, K., Muranyi, W., Glass, B., Laketa, V., Yant, S. R., Tsai, L., Cihlar, T., Müller, B., and Kräusslich, H. G. (2014) Quantitative microscopy of functional HIV post-entry complexes reveals association of replication with the viral capsid. *Elife.* **3,** e04114 Medline
23. Stultz, R. D., Cenker, J. J., and McDonald, D. (2017) Imaging HIV-1 genomic DNA from entry through productive infection. *J. Virol.* **91,** e00034-17 Medline
24. Cihlar, T., and Ray, A. S. (2010) Nucleoside and nucleotide HIV reverse transcriptase inhibitors: 25 years after zidovudine. *Antiviral Res.* **85,** 39–58 CrossRef Medline
25. Loeb, L. A., Essigmann, J. M., Kazazi, F., Zhang, J., Rose, K. D., and Mullins, J. I. (1999) Lethal mutagenesis of HIV with mutagenic nucleoside analogs. *Proc. Natl. Acad. Sci. U.S.A.* **96,** 1492–1497 CrossRef Medline
26. Anderson, J. P., Daifuku, R., and Loeb, L. A. (2004) Viral error catastrophe by mutagenic nucleosides. *Annu. Rev. Microbiol.* **58,** 183–205 CrossRef Medline
27. Venkatesham, A., Pillalamarri, S. R., De Wit, F., Lescrinier, E., Debyser, Z., and Van Aerschot, A. (2019) Propargylated purine deoxynucleosides: new tools for fluorescence imaging strategies. *Molecules* **24,** E468 CrossRef Medline
28. Pauwels, R., Balzarini, J., Baba, M., Snoeck, R., Schols, D., Herdewijn, P., Desmyter, J., and De Clercq, E. (1988) Rapid and automated tetrazolium-based colorimetric assay for the detection of anti-HIV compounds. *J. Virol. Methods* **20,** 309–321 CrossRef Medline
29. Diermeier-Daucher, S., Clarke, S. T., Hill, D., Vollmann-Zwerenz, A., Bradford, J. A., and Brockhoff, G. (2009) Cell type specific applicability of 5-ethynyl-2′-deoxyuridine (EDU) for dynamic proliferation assessment in flow cytometry. *Cytometry A* **75,** 535–546 Medline
30. Ross, H. H., Rahman, M., Levkoff, L. H., Millette, S., Martin-Carreras, T., Dunbar, E. M., Reynolds, B. A., and Laywell, E. D. (2011) Ethynyldeoxyuridine (EdU) suppresses *in vitro* population expansion and *in vivo* tumor progression of human glioblastoma cells. *J. Neurooncol.* **105,** 485–498 CrossRef Medline
31. Neef, A. B, and Luedtke, N. W. (2011) Dynamic metabolic labeling of DNA *in vivo* with arabinosyl nucleosides. *Proc. Natl. Acad. Sci. U.S.A.* **108,** 20404–20409 CrossRef Medline
32. Preston, B. D., Poiesz, B. J., and Loeb, L. A. (1988) Fidelity of HIV-1 reverse transcriptase. *Science* **242,** 1168–1171 CrossRef Medline
33. Roberts, J. D., Bebenek, K., and Kunkel, T. A. (1988) The accuracy of reverse transcriptase from HIV-1. *Science* **242,** 1171–1173 CrossRef Medline
34. Menéndez-Arias, L., Sebastián-Martín, A., and Álvarez, M. (2017) Viral reverse transcriptases. *Virus Res.* **234,** 153–176 CrossRef Medline
35. White, T. A., Bartesaghi, A., Borgnia, M. J., Meyerson, J. R., de la Cruz, M. J., Bess, J. W., Nandwani, R., Hoxie, J. A., Lifson, J. D., Milne, J. L., and Subramaniam, S. (2010) Molecular architectures of trimeric SIV and HIV-1 envelope glycoproteins on intact viruses: strain-dependent variation in quaternary structure. *PLoS Pathog.* **6,** e1001249 CrossRef Medline
36. Brinkman, K., and Kakuda, T. N. (2000) Mitochondrial toxicity of nucleoside analog reverse transcriptase inhibitors: a looming obstacle for long-term antiretroviral therapy? *Curr. Opin. Infect. Dis.* **13,** 5–11 CrossRef Medline
37. Hanes, J. W., and Johnson, K. A. (2008) Exonuclease removal of dideoxycytidine (zalcitabine) by the human mitochondrial DNA polymerase. *Antimicrob. Agents Chemother.* **52,** 253–258 CrossRef Medline
38. Back, D. J., Burger, D. M., Flexner, C. W., and Gerber, J. G.s (2005) The pharmacology of antiretroviral nucleoside and nucleotide reverse transcriptase inhibitors: Implications for once-daily dosing. *J. Acquir. Immune Defic. Syndr.* **39,** S1–S23 CrossRef Medline
39. Ludwig, J. (1981) A new route to nucleoside 5′-triphosphates. *Acta Biochim. Biophys. Acad. Sci. Hung.* **16,** 131–133 Medline
40. Connor, R. I., Chen, B. K., Choe, S., and Landau, N. R. (1995) Vpr is required for efficient replication of human immunodeficiency virus type-1 in mononuclear phagocytes. *Virology* **206,** 935–944 CrossRef Medline
41. He, J., Choe, S., Walker, R., Di Marzio, P., Morgan, D. O., and Landau, N. R. (1995) Human immunodeficiency virus type 1 viral protein R (Vpr) arrests cells in the G_2 phase of the cell cycle by inhibiting p34cdc2 activity. *J. Virol.* **69,** 6705–6711 Medline
42. Szucs, G., Melnick, J. L., and Hollinger, F. B. (1988) A simple assay based on HIV infection preventing the reclustering of MT-4 cells. *Bulletin of the World Health Organization* **66,** 729–737

Design of reverse transcriptase–specific nucleosides to visualize early steps of HIV-1 replication by click labeling

Flore De Wit, Sambasiva Rao Pillalamarri, Alba Sebastián-Martín, Akkaladevi Venkatesham, Arthur Van Aerschot and Zeger Debyser

J. Biol. Chem. 2019, 294:11863-11875.
doi: 10.1074/jbc.RA118.007185 originally published online June 14, 2019